

Soot Formation Study in a Rapid Compression Machine

I. Kitsopanidis

W. K. Cheng

Sloan Automotive Laboratory,
Department of Mechanical Engineering,
Massachusetts Institute of Technology,
77 Massachusetts Avenue,
Cambridge, MA 02139

A rapid compression machine was used to study the soot formation process under diesel enginelike conditions. The apparatus creates accurately controlled conditions at the end of compression (uniform mixture, temperature, and well-defined mixture composition) and, by decoupling chemistry with mixing, provides an unambiguous data interpretation for kinetics study. The soot evolution was studied by the line-of-sight absorption method (at 632.8 nm), which measured the soot volume concentration evolution in the initial stage of soot growth before the optical path became opaque. For a rich butane mixture at fuel equivalence ratio of 3, the ignition delay showed a negative temperature dependence at intermediate temperatures. The soot volume fraction showed an initial exponential growth, with a growth rate depending on the compressed charge fuel concentration. A substantial amount of soot was formed after the soot cloud became opaque. By weighing the total soot particles after the experiment, only ~10–15 % of the soot mass was formed when the beam transmission was reduced to 5%. The final soot mass was ~15–18 % of the total carbon mass for compressed charge density of 250 mol/m³ and temperature from 740 to 930 K. [DOI: 10.1115/1.2180279]

Introduction

Airborne particulate matter (PM) is a major air-quality concern because of its health effects and its impact on visibility [1]. As a result, the U.S. Environmental Protection Agency has established strict standards for the atmospheric PM levels [2]. A substantial source of PM in urban areas is vehicles, especially those powered by diesel engines. The PM emission from diesel engines originate from soot particles generated during the combustion process. These particles serve as condensation nuclei for low vapor pressure exhaust species, such as unburned or partially burned fuel and engine oil, where the particles grow further in mass [3]. Therefore, to effectively control PM emissions, it is important to understand the processes by which soot is formed in combustion.

Much of the current understanding of diesel combustion process was obtained from optical engine studies, such as those done at the Sandia National Laboratory [4]. Figure 1 shows a schematic of the combusting fuel jet. There are two major characteristics that are pertinent to the soot formation process:

1. *The fuel goes through a two-stage oxidation process.* The first stage is in the fuel-rich premixed zone just downstream of the liquid spray; then the products of this fuel-rich combustion are oxidized in the diffusion flame at the periphery of the plume.
2. *Soot is first formed in the fuel-rich premixed zone where fuel-air equivalence ratio (Φ) is in the range of 2–4.* Soot then grows in the environment of high-temperature fuel-rich combustion products by surface growth and agglomeration as it is convected toward the end of the plume.

Thus, soot formation is governed by the chemistry of the premixed fuel-rich mixture at Φ values of 2–4.

There are two classes of diesel soot formation studies:

- (a) The observation of the process in a fuel jet that undergoes evaporation, mixing, ignition, and burning processes. The experiment could be done in an actual diesel engine, in a constant volume combustion vessel, in a burner, or in a

rapid compression machine (RCM) [5–12]. Although the process is realistic in these studies, it is difficult to extract quantitative kinetics information on soot formation because of the inherent nonuniformity and uncertainties in species concentrations and temperatures.

- (b) The study of a reacting premixed mixture. The reaction is initiated by a shock wave in a shock tube, or by rapid compression in a rapid compression machine. In these studies, the operating environment is well controlled and quantitative data can be obtained for soot formation rates.

Data on soot formation rate and yield under premixed fuel-rich conditions have been obtained in shock tube studies at pressure and temperatures comparable to those found in diesel combustion [13–15]. Because of the low specific heat ratio of a fuel-rich hydrocarbon mixture, however, the shock tube studies were customarily done under heavily diluted conditions with a mixture consisting of 95–99.5 % argon so as to produce the correct thermal environment. As a result, the species concentrations were unrealistically low, and there was negligible heat release from the mixture in the process. To create a thermal and species concentrations environment that is representative of diesel combustion, rapid compression of a homogeneous fuel-rich mixture in an RCM is employed in this study.

The RCM is a single-stroke device which rapidly compresses a uniform mixture of fuel and air. The piston is locked at the end of the stroke to produce constant volume combustion. Figure 2 summarizes the temperature and fuel carbon concentration (in the combustible mixture) regimes of various experimental setups. It is apparent that the temperature and fuel carbon conditions achieved in an RCM are much more representative of those found in the soot formation process in a diesel engine compared to all other alternatives.

Soot detection in a combustion process can be achieved either with direct sampling or optical techniques. Molecular beam sampling combined with electron microscopy has been successful in identifying critical intermediates in burner types of experimental setups. Though sampling methods have been used directly in diesel engines [6], they are intrusive and it is difficult to obtain time-resolved data using the technique. The advancement of laser technology, on the other hand, made available nonintrusive tools for combustion diagnostics. The most common optical methods used for soot detection are the line-of-sight (LOS) absorption [7–11]

Contributed by the Internal Combustion Engines Division of ASME for publication in the JOURNAL OF ENGINEERING FOR GAS TURBINES AND POWER. Manuscript received July 11, 2005; final manuscript received October 24, 2005. Review conducted by M. Wooldbridge.

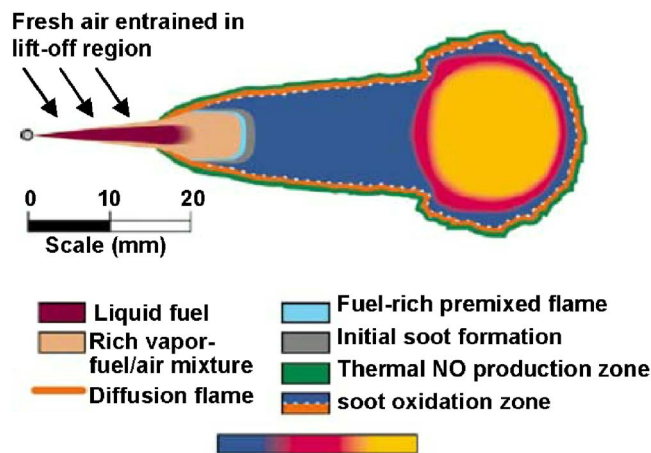


Fig. 1 Schematic of a diesel fuel spray illustrating the combustion processes [4]

and laser induced incandescence (LII) [12]. The latter method, however, could not provide the time resolution required for the single-shot RCM experiment. Therefore, LOS absorption was used to monitor the soot formation process.

The aim of the present work is to demonstrate the ability to study soot formation under diesel engine-like conditions created in an RCM using the LOS absorption technique. The RCM, which provides well-controlled conditions (pressure, temperature, and mixture composition), along with the nonintrusive technique of LOS absorption, are tools that could shed light on soot formation and provide valuable data for chemical kinetics modeling efforts.

Rapid Compression Machine

The RCM is a single-stroke device, which rapidly compresses a uniform mixture of fuel and oxidant to conditions similar to diesel engine operation. In contrast to an engine, the piston of the current RCM is locked in the compressed position to produce a constant volume environment. The mixture remains at these conditions for a longer period of time compared to a shock tube (~ 10 ms versus ~ 1 ms); this time is only limited by heat losses. Thus, the thermal and composition conditions of the mixture under study are well defined.

The RCM, shown in Fig. 3, has a cylindrical combustion chamber with 5.08 cm bore and 1.27 cm clearance height. The piston starting position can be adjusted by changing the effective length of the hydraulic chamber with spacers (not shown in Fig. 3). The compression stroke then ranges from 15.24 cm to 20.32 cm, resulting in a compression ratio between 12.5 and 16.5. These values have taken into account the 3.1% crevice volume (compared to the clearance volume) in the piston and windows at the end of

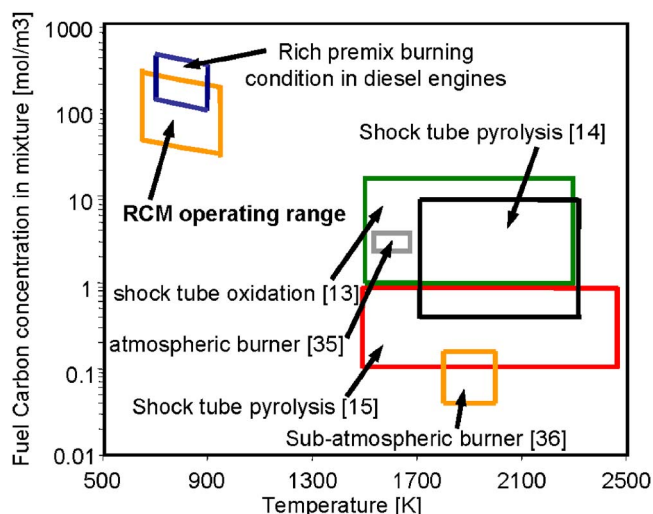


Fig. 2 Conditions for soot formation in diesel engines and in various experimental studies

compression. For the data shown in this paper, the compression ratio was set to 16.5. The geometry and dimension of the current machine is comparable to others in the literature [16–18].

The piston is pneumatically driven and uses a pin-and-groove mechanism in a hydraulic chamber to decelerate the piston at the end of the stroke [19]. In its retracted position, the pneumatic piston is pressurized (from the right of Fig. 3) to 17.5 bar gage pressure by a large tank of nitrogen, but it is locked in position by the high-pressure oil (at 90 bar gage pressure) in the hydraulic chamber. When the oil pressure is released by a small solenoid valve, the piston moves forward, and thereby releases the locking hydraulic piston and starts the compression process.

During much of the stroke, the piston accelerates almost freely since the friction forces of the seals and oil are modest, and the pressure rise in the combustion chamber is not yet significant. The piston starts to decelerate significantly when the “pin” on the hydraulic piston enters the groove near the end of the stroke. The clearance between the pin and the groove is only 0.7 mm so that there is a large back pressure buildup that is responsible for stopping the piston with a reasonable cushion.

The calculated piston velocity and combustion chamber pressure (p) are shown in Fig. 4. The piston motion was obtained by using Newton’s law; the substantial resistances to motion were the pressure buildup in the combustion chamber and the significant back pressure when the pin hit the groove. The latter value was obtained by a simple one-dimensional (1D) viscous flow calculation. The peak piston velocity was more than 30 m/s, and the total compression time was 15 ms. The effective compression time (de-

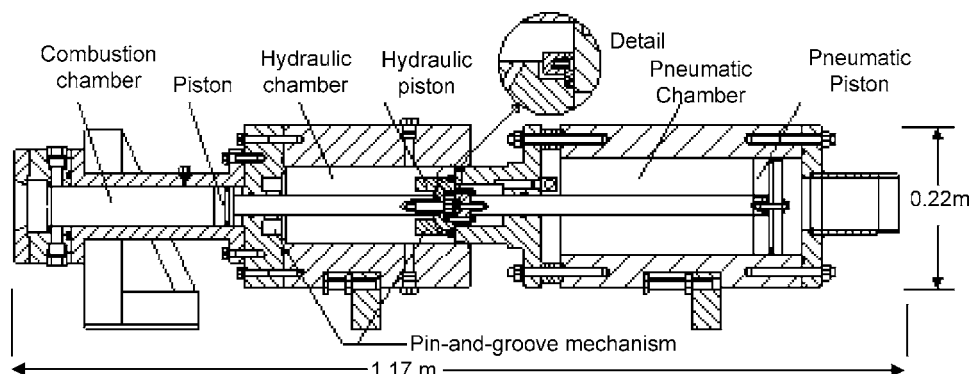


Fig. 3 Schematic of the rapid compression machine

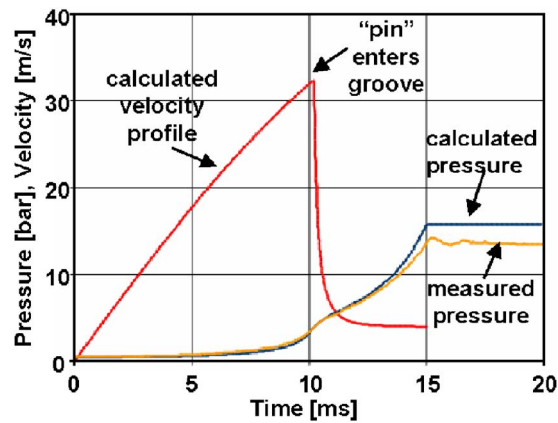


Fig. 4 Calculated piston velocity and comparison of calculated and observed pressure traces. *N*-butane/oxygen/argon mixture; $\text{Ar}/\text{O}_2=3.773$, $\Phi=3$; precompression pressure and temperature: 0.4 bar, 49°C.

fined as $p/(dp/dt)$ at the inflection point of the pressure trace) was 4 ms. The final compression time (defined as $p/(dp/dt)$ at the end of compression) was 0.4 ms. The calculated pressure (from adiabatic compression) agrees well with the experimental value except at the end of compression because of heat transfer. Because of the high deceleration (~ 3000 g) when the pin enters the groove, the finite impact velocity (~ 5 m/s) at the end of the stroke, and the large moving mass (6 kg), it is necessary to substantially anchor the RCM to prevent significant vibrations.

After reaching its final compression point, the piston was kept in place by the high-pressure driving gas so that constant volume combustion can be realized. For the driving pressure of 17.5 bar, the piston can hold a maximum combustion chamber pressure of 110 bar with the designed area ratio of the driving and the combustion chamber pistons.

The combustion chamber is equipped with four fused silica windows 1.27 cm dia around the circumference of the combustion chamber for line of sight measurements and a fully transparent cylinder head for imaging studies. Because the compression is rapid, the heat transfer to the wall is limited to a thin boundary layer so that there is a substantial adiabatic core in the charge. Then the compression temperature (T_{comp}) of this core may be obtained from the measured compression pressure (P_{comp}) and the initial condition (P_{ini} and T_{ini}) via the isentropic relation

$$\int_{T_{\text{ini}}}^{T_{\text{comp}}} c_p(T) \frac{dT}{T} = R \ln \left(\frac{P_{\text{comp}}}{P_{\text{ini}}} \right) \quad (1)$$

Here, $c_p(T)$ is the heat capacity per mole of the mixture at temperature T , and R is the universal gas constant. A Kistler 6125A piezoelectric pressure transducer was used to measure the combustion chamber pressure at sampling frequency of 100 kHz.

The mixture was prepared manometrically. The combustion chamber was evacuated before the gaseous mixture components were introduced. A Baratron 622A pressure transducer with accuracy of 0.1 Torr was used to meter each mixture component. The combustion chamber, connecting lines and fuel reservoirs were all insulated, heated, and temperature controlled to accommodate nonvolatile fuels, which required an initial temperature to be higher than the highest dew point corresponding to the partial pressure of the respective component in the mixture.

To obtain high compression temperatures, an argon/oxygen mixture was used instead of air as the oxidant. The Ar/O_2 molar ratio was fixed at 3.773, which is the same as the N_2/O_2 ratio in air. Then, at the end of compression, a relatively wide range of conditions similar to the range found in diesel engines

(10–30 bar, 700–900 K) was accomplished by varying the initial temperature and pressure before compression commenced.

After each run, the soot in the combustion chamber was collected and weighed, although there might still be trace amount of soot left on the O-rings and crevices. Then the combustion chamber, window, and piston surfaces were cleaned with acetone. Special care was taken at the crevices where soot could accumulate. Then all O-rings were cleaned with acetone, dried, and lubricated with vacuum grease before reassembly. The piston ring was cleaned only after every 20 runs because the procedure involved substantial disassembly of the apparatus. After the apparatus was reassembled, the combustion chamber was heated to the desired temperature and evacuated before the new mixture was introduced. Because of the high vapor pressure of acetone (normal boiling point 56.6°C), there should not be any substantial solvent materials left after the system was pumped down.

Laser Extinction Measurement of Soot Volume Concentration

Real-time line-of-sight (LOS) absorption using a helium-neon laser beam at a wavelength (λ) of 632.8 nm is used to determine the soot volume concentration evolution. The method is well established [20,21] and briefly summarized as follows.

Since the soot particle sizes at the nucleation and initial growth stages are less than, or of the order of, 50 nm [21–23], which is much less than λ/π , the interaction of the particles and the light beam is in the Rayleigh regime; the extinction of the laser beam is predominantly due to absorption rather than scattering. Assuming that the particles are spherical with diameter D , the absorption cross section is proportional to D so that the extinction coefficient is proportional to D^3 and, hence, proportional to the soot particle volume. Then the attenuation of the laser beam may be related to the LOS integral of the soot volume fraction

$$\ln \left(\frac{I}{I_0} \right) = \frac{6\pi}{\lambda} \text{Im} \left(\frac{m^2 - 1}{m^2 + 2} \right) \int_0^L f_v dx \quad (2)$$

In Eq. (2), I_0 and I are the incident and transmitted laser beam intensities, m is the complex refractive index of the soot particles, L is the path length, and the soot volume concentration f_v is defined by

$$f_v = n \int_0^\infty \frac{\pi D^3}{6} p(D) dD \quad (3)$$

where n is the soot particle number per unit volume and $p(D)$ is the probability distribution of the particle diameter. If the soot cloud is uniform in space, the value of f_v may be obtained from the measurement of I/I_0 as

$$f_v = \frac{\lambda \ln(I/I_0)}{6\pi L \text{Im} \left(\frac{m^2 - 1}{m^2 + 2} \right)} \quad (4)$$

It is assumed that the refractive index m is known and remains constant during the course of soot evolution. The refractive index of soot has only been determined in the bulk. Chang and Charalampopoulos [24] measured the complex refractive index based on dynamic light scattering at a wavelength of 632.8 nm to be $1.8-0.58i$ at 10 mm above the burner surface and $1.62-0.47i$ at 6 mm. Lee and Tien [25] calculated the complex refractive index based on the multivariable dispersion model to be $1.9-0.55i$ at 632.8 nm without finding any significant temperature effect. The maximum difference in the calculated soot volume concentration using any of the above values is $\pm 6\%$. To be consistent with most recent studies, the value suggested by Chang and Charalampopoulos at 10 mm above the burner was used in this study.

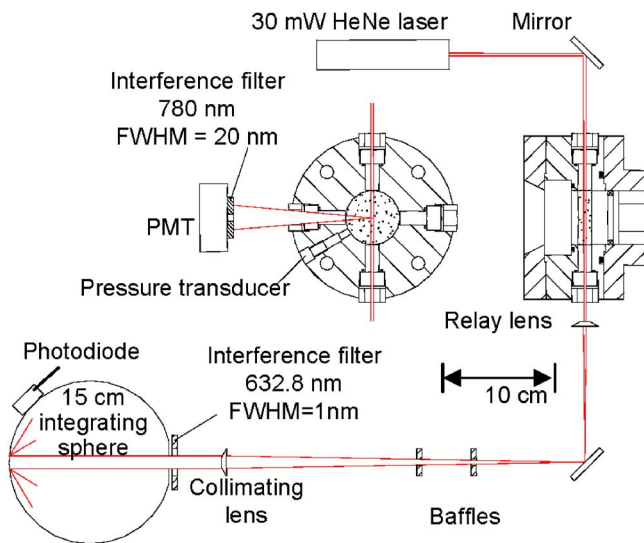


Fig. 5 Schematics of optical setup

Optical Setup. The schematic of the optical setup is shown in Fig. 5. A 30 mW He–Ne laser beam passes through the combustion chamber, where it is attenuated by fuel-rich combustion generated soot particles. The attenuated beam is then connected to the photodiode detector at a rather large distance (~ 0.6 m) by relay lenses, baffles, and spectral filter.

The above optical arrangement is necessary because there is a significant amount of combustion-generated light. During combustion, light emission takes place due to chemiluminescence and soot luminosity. The former arises from radicals decaying back to equilibrium energy levels after being raised to an excited energetic state. In hydrocarbon oxidation, such species are OH (310 nm), C_2 (516 nm), CH_2O (368–470 nm), and especially CH (390, 430 nm) [26]. Dec and Espey, after conducting experiments in a diesel engine, found that chemiluminescence peaks at around 430 nm and is almost zero above 620 nm, with HCO speculated as the only possible species responsible at higher wavelengths [27]. By using a laser light at 632.8 nm, the chemiluminescence interference can be eliminated. Soot luminosity, on the other hand, arises from soot particles, which act as radiating gray bodies after being generated. The emission of this light has a broadband spectrum, and for typical rich combustion temperatures of 1800–2000 K, the emissive power can be significant at 632.8 nm. The level is comparable to that of the laser light during the later stage of combustion since the latter is strongly attenuated by the soot particles.

To minimize soot luminosity detected by the photodiode, a narrow band (FWHM of 1 nm) interference filter was used and the detector was moved away from the test section, since the soot luminosity contribution drops with the square of distance. The signal improvement is shown in Fig. 6, in which the detected signals under the same compression conditions are compared. Curve A shows the transmission signal with the optical setup of Fig. 5; curve B shows the one obtained with photodiode and interference filter at ~ 5 cm from the combustion chamber window. The significantly higher apparent transmission in curve B is due to the contribution from soot emissions. Experiments were also run with the optical arrangement of Fig. 5 with the laser beam off. No luminosity was detected; thus, the arrangement was sufficient to reduce the soot luminosity contribution to a negligible level.

With a long optical path, significant noise is induced at the detector due to beam wander. The beam motion is caused by mechanical vibrations of the optical train and by beam steering due to the refractive index gradients inside the combustion chamber. To alleviate these effects, an integrating sphere is used to collect

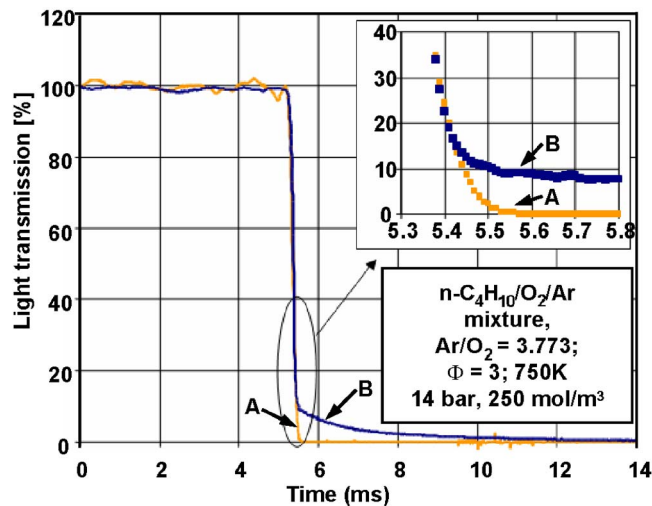


Fig. 6 Effect of soot luminosity on apparent transmission: (a) signal with optical arrangement of Fig. 5 and (b) with detector and filter at 5 cm from combustion chamber window

the laser light so that the detector signal is not sensitive to beam wander. Note also that since the interference filter is partial to the angle of incidence, it has to be placed in front of the integrating sphere; a collimating lens is further used to direct the whole beam at normal incidence to the filter.

Confirmation of Absorption Signal due to Soot Particles.

There are reports in the literature that query whether light absorption at 632.8 nm is evidence of soot particles presence. Microscopy studies suggest that there are large molecules other than soot particles that may absorb light at this wavelength [28]. Other studies suggested that very young soot particles may not absorb light at this wavelength [29,30]. Though the distinction between soot precursors (which are large molecules) and soot particles is arbitrary; there does not seem to be any gaseous species (i.e., molecules that are not large enough to exhibit macroscopic properties, such as black-body radiation) that absorb light at 632.8 nm [31]. Then absorption at this wavelength may be interpreted as an indication of soot presence. To confirm this point, a photomultiplier tube (PMT) was placed above the top window of the RCM with an interference filter at 780 nm (FWHM (full width at half maximum) = 10 nm), as shown in Fig. 5. Laser light scattering is blocked by the filter, and, as already explained earlier, there is no chemiluminescent at this wavelength. Thus, the only light that can be detected by this PMT comes from particle gray-body radiation, which indicates the presence of a “particle.” Figure 7 shows the PMT detected signal and the light transmission simultaneously. The luminosity signal starts at the same time as light absorption. This fact confirms that the absorbing media is indeed in the particulate phase.

Results

In the following, typical results from the RCM are used to demonstrate the performance of the machine and the type of data it provides. Comprehensive data sets and comparison of data with models of ignition delay and soot formation kinetics will be presented in later publications.

Figure 8 shows the pressure trace and light transmission for five consecutive tests of a typical fuel-rich mixture. All tests were conducted with *n*-butane/ O_2 /Ar mixture, at $Ar/O_2 = 3.773$ and $\Phi = 3$. The conditions at the end of compression were the same for all tests: $P_{comp} = 14$ bar, $T_{comp} = 765$ K, and total molar concentration $n_{comp} = 250$ mol/ m^3 . After a total compression time of ~ 15 ms, there is a period of preignition reaction, during which the rate of heat release cannot keep pace with the heat losses and

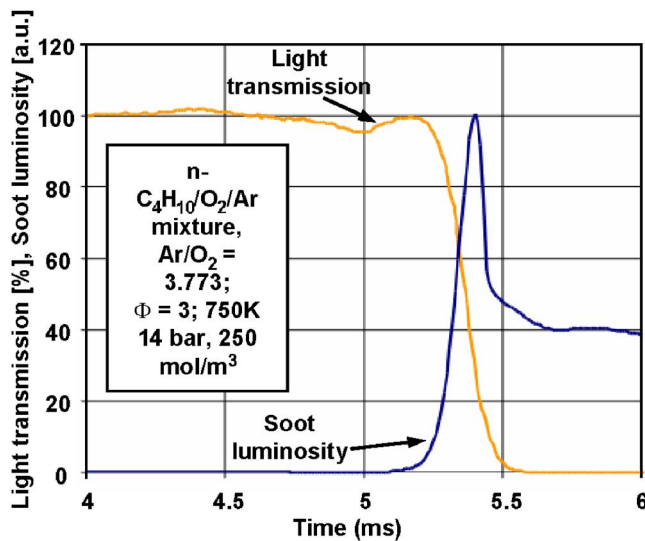


Fig. 7 Soot luminosity and light transmission

the pressure drops slightly before the mixture ignites at ~ 8 ms after the end of compression. The heat release is in two stages, with a slower rate first followed by a rapid one. These observations are consistent with what is reported in the literature for most hydrocarbon fuels [32]. The pressure drop from the peak value is due to heat transfer to the cold walls when the combustion is over. Note that the repeatability is excellent for both the pressure trace and the light transmission; for example, the variability of the ignition delay is ± 0.15 ms at 95% confidence level.

Ignition Delay and Combustion Time. The ignition delay and combustion time may be derived from the pressure curve as illustrated in Fig. 9. The ignition delay is defined as the time from the end of compression to the time at the 10% heat release point. To assess the combustion rate, the 5–20% and the 20–80% burn duration are chosen to reflect the early and later parts of combustion. The threshold levels used in these definitions are somewhat arbitrary but are chosen to give well-defined results. (For example, because of the uncertainty in the heat release curve, the 80% heat release point is much better defined than the 90% one.) Although the main purpose of the experimental study is on soot formation,

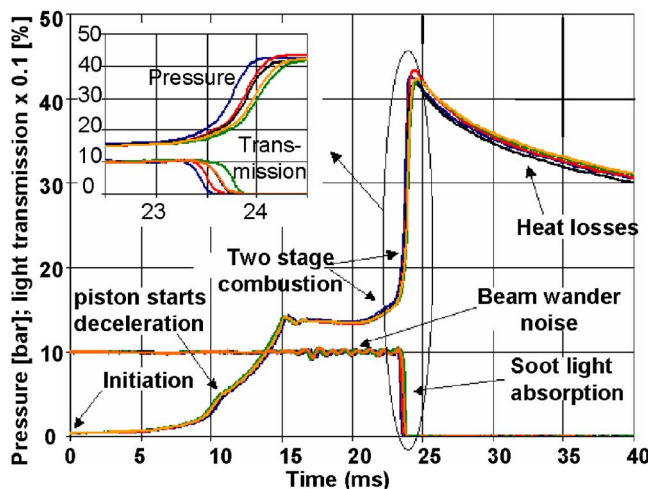


Fig. 8 Repeatability of data; five repeats. *N*-butane/oxygen/argon mixture; $\text{Ar}/\text{O}_2=3.773$, $\Phi=3$; compressed conditions: 750 K, 14 bar, 250 mol/m³.

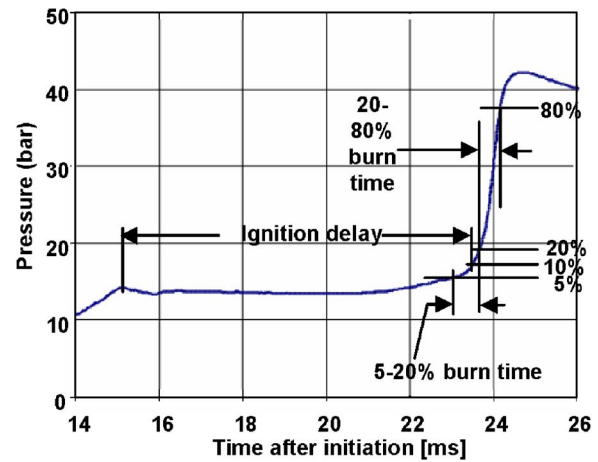


Fig. 9 Ignition delay and combustion times. *N*-butane/oxygen/argon mixture; $\text{Ar}/\text{O}_2=3.773$, $\Phi=3$; compressed conditions: 765 K, 14 bar, 250 mol/m³.

the ignition delay, and the combustion times are essential for validating the chemical kinetics of the soot formation process. These values are also archival since there is not very much fundamental data on ignition delay and combustion times for hydrocarbon fuels under fuel-rich conditions.

The ignition delay data for *n*-butane at fuel equivalence ratio (Φ) of 3 and a compression molar density of 250 mol/m³ are shown in Fig. 10. Note that to vary the compression temperature, the set of experiments was done at different initial temperatures; the initial pressures were adjusted to produce the same compression molar density. The Arrhenius plot is typical of data from hydrocarbons: at low temperatures, the ignition delay decreases rapidly with increase of temperature. At intermediate temperatures, the delay stays fairly constant or even increases slightly because of the well-known negative temperature coefficient (NTC) regime of the chemistry involved. At higher temperatures, the delay decreases again with increase in temperature. The repeatability of the ignition delay value is $\pm 2\%$.

The 5–20% and 20–80% burn times are plotted in Fig. 11. The early burn time followed an Arrhenius temperature dependence with activation energy of 3.38 kcal/mol. Both values are of the order of a fraction of 1 ms. The repeatability of the burn times is $\pm 12\%$.

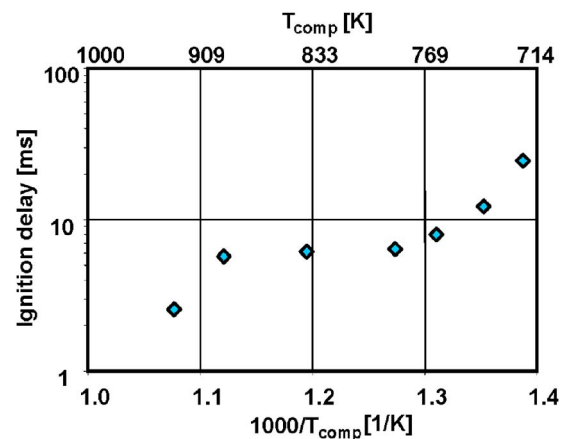


Fig. 10 Ignition delay as function of compression temperature. *N*-butane/oxygen/argon mixture; $\text{Ar}/\text{O}_2=3.773$, $\Phi=3$; compressed molar density: 250 mol/m³.

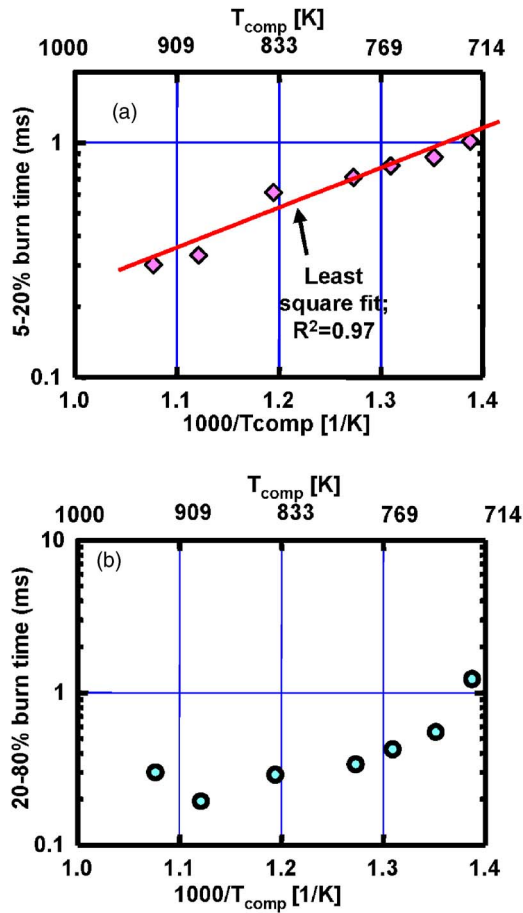


Fig. 11 Combustion time as a function of compression temperature: (a) 5–20 % burn time and (b) 20–80 % burn time. *N*-butane/oxygen/argon mixture; $\text{Ar}/\text{O}_2=3.773$, $\Phi=3$; compressed molar density: 250 mol/m^3 .

Soot Evolution. The instantaneous soot volume concentration f_v may be calculated the transmission signal according to Eq. (4). Because of the beam wander noise (see Fig. 8) and that the signal-to-noise ratio was not favorable at high beam attenuation, the signal was only deem valid when the transmission was between 90% and 5%. It should be noted that the 5% transmission point does not mark the end of soot formation. Since the mixtures are sufficiently rich, the combustion chamber can become almost opaque well before the soot formation process ends. Collecting and weighing the soot after the end of the experiment and converting the mass to an equivalent final soot volume concentration (using a nominal density of 1.8 g/cm^3), it was found that, depending on the operating conditions, the value of f_v at the 5% transmission point corresponds to only 10–15 % of the final value. The absorption experiments, therefore, only provide information about the initial stage of soot formation. This information, however, is critical for validating the soot formation kinetics.

The time evolutions of the soot volume concentration are shown in Fig. 12, in which the value of f_v is normalized by the molar concentration of carbon atoms at end of compression (denoted by $[C]_{\text{comp}}$) to obtain a soot yield (SY). Specifically, the definition of SY is

$$\text{SY} = \frac{\rho_s f_v}{W_C [C]_{\text{comp}}} \quad (5)$$

where $\rho_s=1.8 \text{ g/cm}^3$ is the presumed density of soot, $W_C=12 \text{ g/mol}$ is the atomic weight of carbon, and $[C]_{\text{comp}}$ is the molar carbon concentration of the charge at end of compression.

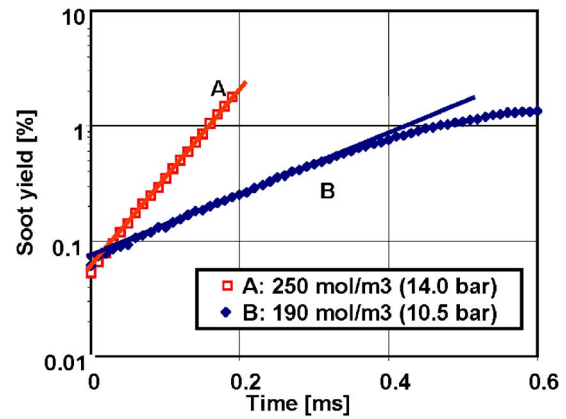


Fig. 12 Soot formation history at two different gas densities. *N*-butane/oxygen/argon mixture; $\text{Ar}/\text{O}_2=3.773$, $\Phi=3$; compressed temperature: 765 K . Time zero corresponded to point of 90% light transmission.

The time zero corresponded to the point of 90% transmission, while the end point corresponded to 5% transmission. For the data in case A (at $\Phi=3$, compression temperature and density of 765 K and 250 mol/m^3), SY grew exponentially in time. For case B (same condition as case A, except that the compressed density was lower, at 190 mol/m^3), the exponential growth was observed for the initial part of the trace. The growth rate was then slower at a later time. The initial exponential growth was observed in all the test cases with Φ ranging from 2.5 to 4.5 over a large range of compression temperatures and densities.

The empirically observed exponential growth of SY cannot be simply explained. If it is assumed that in this period, the particles are predominantly in the growth stage (i.e., nucleation is complete and agglomeration is not yet important so that the particle number density (n) is approximately constant), then the growth of soot particle is governed by the condensation of the gaseous hydrocarbon (HC) species, such as polycyclic aromatic hydrocarbons (PAH) and C_2H_2 , derived from the fuel molecules. These species have a higher C/H ratio than the parent molecule; they act as building materials to the surface growth of the young soot particles [33]. For a spherical soot particle of diameter D that is smaller than the mean free path, the growth in volume should then be proportional to the collision area

$$\frac{d}{dt} \left(\frac{\rho \pi D^3}{6} \right) = \frac{(\pi D^2)}{4} [\text{HC}] W_{\text{HC}} v_{\text{HC}} \quad (6)$$

where ρ is the density of the soot particle, $[\text{HC}]$ and W_{HC} are the molar concentration and molecular weight of the condensing soot precursors, and v_{HC} is the relative velocity between the precursor molecules and the soot. If the values of ρ , $[\text{HC}]$, W_{HC} , and v_{HC} are constant, the soot volume concentration f_v , which is proportional to nD^3 , should, according to Eq. (6), increase as t^3 , which is much slower than exponential.¹

Since the soot particles are known to be porous, one may make the tacit assumption that the density decreases as the particle grows, where $\rho \propto 1/D$. Then D grows exponentially in time and the soot yield (SY) is:

$$\text{SY} \propto \exp\{(a W_{\text{HC}} v_{\text{HC}}) [\text{HC}] t\} \quad (7)$$

where a is a proportional constant. Thus, the growth rate would be proportional to the precursor concentrations $[\text{HC}]$. Equation (7)

¹At a charge density of $\sim 200 \text{ mol/m}^3$, the mean free path is $\sim 10 \text{ nm}$. The large particles may approach the continuum limit. Then the growth rate is proportional to $t^{3/2}$, which is even slower.

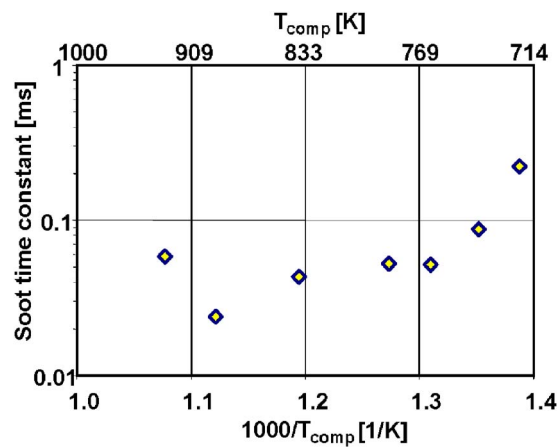


Fig. 13 Soot formation time constant as a function of compression temperature. *N*-butane/oxygen/argon mixture; $Ar/O_2 = 3.773$, $\Phi = 3$; compressed molar density: 250 mol/m^3 .

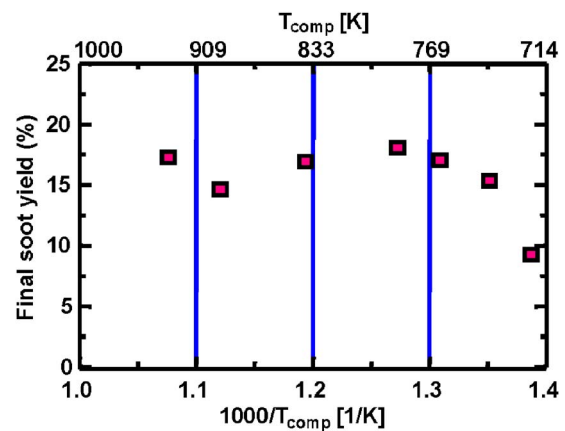


Fig. 14 Final soot yield as a function of temperature. *N*-butane/oxygen/argon mixture; $Ar/O_2 = 3.773$, $\Phi = 3$; compressed molar density: 250 mol/m^3 .

explains qualitatively the features in Fig. 12:

- The growth is exponential in time,
- The slope of the plotted lines increases with charge density increase, which supplies a higher value of [HC].
- For Case B, which has a lower charge density, the growth rate at a later time is slower than exponential because of the depletion of [HC]. (Similar behavior was not observed in case A because the optical path had become opaque before the slow down in the growth rate.)

Quantitative, however, it is much more difficult to reach agreement. We expect that [HC] should be proportional to the amount of fuel present, so the growth rate should be proportional to the fuel concentration (which, for fixed Φ value, scales with the compressed charge density). Experimentally, the ratio of the two slopes in Fig. 12 is 2.90; this value disagrees with the ratio of the charge density at end of compression: ratio = $250/190 = 1.32$. Thus, the dependence on the fuel concentration is complex and there is no simple closure. Quantitative comparisons could only be sought through detailed modeling of the formation and oxidation of both the precursors and soot [34].

Since the observed initial growth of the soot volume concentration is exponential, a soot formation time constant (equal to the inverse of the logarithmic soot yield growth rate) may be obtained. The time constant is shown in Fig. 13 as a function of compression temperature at $\Phi = 3$ and compression density of 250 mol/m^3 . The values are below 0.1 ms at compression temperatures above 740 K.

Final Soot Yield. As mentioned before, the soot cloud becomes opaque as time progresses so that the LOS absorption measurement could not provide information about the later part of the soot evolution process. The total final soot mass, however, could be obtained by carefully collecting all the soot particles from the inside of the apparatus after the experiment and weighing them with a microbalance (Ohaus Model EP214 with resolution of 0.1 mg). Depending on the experimental condition, the collected soot mass was of the order of 5–30 mg. In spite of the crudeness of the method, repeatability was excellent; the uncertainty was $\pm 5\%$ (based on five repeats). The final soot yield (total final soot mass normal by total mass of carbon atoms in the combustion chamber) for a mixture at $\Phi = 3$, and compressed charge density of 250 mol/m^3 is plotted in Fig. 14 as a function of temperature. Except for the experiment at the lowest temperature (722 K), the final soot yield at these conditions is not sensitive to temperature (740–930 K); the value is $\sim 15\text{--}18\%$.

Conclusions

The rapid compression machine (RCM) was demonstrated to be an appropriate apparatus for studying soot formation under fuel-rich conditions in an environment similar to that in actual diesel engines. Unlike engines studies, however, the RCM provides a uniform charge with well-defined temperature and pressure so that the results can be interpreted quantitatively. Unlike shock tube studies, the fuel/air mixture is not diluted so that soot formation process can be studied under realistic levels of fuel carbon concentrations. The soot volume concentration evolution was observed in real time by line-of-sight absorption measurement at 632.8 nm. Luminosity from the soot radiation interfered with the measurement; the interference was alleviated by placing the detector far from the test section and the use of baffles and a narrowband pass-interference filter. Data were reported from compression ignition of a *n*-butane/oxygen/argon mixture with argon to oxygen molar ratio of 3.773 (equal to that of nitrogen to oxygen ratio in air) under fuel-rich condition at a fuel equivalence ratio of 3. The ignition delay versus temperature data showed a negative temperature coefficient region at intermediate temperatures. The combustion was in two stages: a slower one followed by a rapid one.

For all the experiments, the instantaneous volume concentration grew exponentially in time, initially. When the fuel concentration of the compressed charge was sufficiently low, slower growth rate was observed in a later stage before the soot cloud became opaque. There was, however, no simple model that would explain the initial exponential growth behavior. The time constant associated with this growth was fast—less than 0.1 ms for temperatures above 740 K at fuel equivalence ratio of 3 and charge density of 250 mol/m^3 . There was significant further soot formation after the laser beam was blocked by the soot cloud. The soot concentration at 5% transmission was $\sim 10\text{--}15\%$ of the final soot concentration obtained by weighing the soot particles collected from the combustion chamber after the experiment. The final soot mass was $\sim 15\text{--}18\%$ of the carbon mass in the charge.

Acknowledgment

This work was supported by the Center of Airborne Organics of the U.S. Environmental Protection Agency, and an Industrial Consortium for Engine and Fuels Research. The members of the Consortium were DaimlerChrysler, Delphi, ExxonMobil, Ford Motor, and GM. I. Kitsoponidis was also supported by a fellowship from Cummins Engine Co.

References

- [1] U.S. Environmental Protection Agency, 1966, "EPA's Proposal for the Particulate Matter Standard: Fact Sheet."
- [2] Anon, 1997, "National Ambient Air Quality Standards for Particulate Matter; Final Rule," Federal Register, 62, p. 38652.
- [3] Heywood, J. B., 1988, *Internal Combustion Engine Fundamentals*, McGraw-Hill, New York.
- [4] Dec, J., 1997, "A Conceptual Model of DI Diesel Combustion Based on Laser-Sheet Imaging," SAE Paper No. 970873.
- [5] Senda, J., Choi, D., Iwamuro, M., Fujimoto, H., and Asai, G., 2002, "Experimental Analysis on Soot Formation Process in DI Diesel Combustion Chamber by Use of Optical Diagnostics," SAE Paper No. 2002-01-0893.
- [6] Pungs, A., Pischinger, S., Backer, H., and Lepperhoff, G., 2000, "Analysis of the Particle Size Distribution in the Cylinder of a Common-Rail DI Diesel Engine During Combustion and Expansion," SAE Paper No. 2000-01-1999.
- [7] Tree, D., and Dec, J., 2001, "Extinction Measurements of In-Cylinder Soot Deposition in a Heavy Duty DI Diesel Engine," SAE Paper No. 2001-01-1296.
- [8] Song, K. H., Lee, Y., and Litziger, A., 2000, "Effects of Emulsified Fuels on Soot Evolution in an Optically Accessible DI Diesel Engine," SAE Paper No. 2000-01-2794.
- [9] Hentschel, W., and Richter, J. U., "Time Resolved Analysis of Soot Formation and Oxidation in a Direct-Injection Diesel Engine for Different EGR Rates by an Extinction Method," SAE Paper No. 952517, 1995.
- [10] Wiartalla, A., Backer, H., and Durnholz, M., "Influence of Injection System Parameters on Spray Development, Combustion and Soot Formation by Optical Measurement Techniques in a Model Combustion Chamber," SAE Paper No. 950233, 1995.
- [11] Miysmoto, N., Ogawa, H., Goto, N., and Sasaki, H., "Analysis of Diesel Soot Formation Under Varied Ignition Lag With a Laser Light Extinction Method," SAE Paper No. 900640, 1990.
- [12] Dec, J., and Espey, C., "Ignition and Early Soot Formation in a DI Diesel Engine Using Multiple 2D Imaging Diagnostics," SAE Paper No. 950456, 1995.
- [13] Kellerer, H., Koch, R., and Wittig, S., 2000, "Measurements of the Growth and Coagulation of Soot Particles in a High-Pressure Shock Tube," *Combust. Flame*, **120**, pp. 188–199.
- [14] Bauerle, S., Karasevich, Y., Slavov, S., Tanke, D., Tappe, M., Thienel, T., and Wagner, H. G., 1994, "Soot Formation at Elevated Pressures and Carbon Concentrations in Hydrocarbon Pyrolysis," *25th Symposium (International) on Combustion*, The Combustion Institute, Pittsburgh, pp. 627–634.
- [15] Parker, T. E., Foutter, R. R., and Rawlins, W. T., 1990, "Soot Initiation and Particle Growth in the Pyrolysis of Toluene at High Inert Gas Pressures," *AIP Conf. Proc.*, **208**, pp. 481–486.
- [16] Griffiths, J. F., Jiao, Q., Kordylewski, W., Schreiber, M., Meyer, J., and Knoche, K. F., 1993, "Experimental and Numerical Studies of Di-tert-butyl Peroxide Combustion at High Pressures in a Rapid Compression Machine," *Combust. Flame*, **93**, pp. 303–315.
- [17] Carlier, M., Corre, C., Minetti, R., Pauwels, J. F., Ribaucour, M., and Sochet, L. R., 1990, "Autoignition of Butane: A Burner and a Rapid Compression Machine Study," *23 Symposium (International) on Combustion*, The Combustion Institute, Pittsburgh, pp. 1753–1758.
- [18] Park, P., and Keck, J. C., 1990, "Rapid Compression Machine Measurements of Ignition Delays for Primary Reference Fuels," SAE Paper No. 900027.
- [19] Affleck, W. S., and Thomas, A., 1968, "An Opposed Piston Rapid Compression Machine for Pre-Flame Reaction Studies," *Proc. Inst. Mech. Eng.*, **183**, pp. 365–381.
- [20] Jones, A. R., 1999, "Light Scattering for Particle Characteristics," *Prog. Energy Combust. Sci.*, **25**, pp. 1–53.
- [21] Haynes, B. S., and Wagner, H. G., 1981, "Soot Formation," *Prog. Energy Combust. Sci.*, **7**, 229–273.
- [22] Graham, S. C., 1976, "The Collisional Growth of Soot Particles at High Temperatures," *16th Symposium (International) on Combustion*, The Combustion Institute, Pittsburgh, pp. 663–669.
- [23] Amann, C. A., and Siegl, D. C., 1982, "Diesel Particulates—What They Are and Why?," *Aerosol Sci. Technol.*, **1**, pp. 73–101.
- [24] Chang, H., and Charalampopoulos, T. T., 1990, "Determination of the Wavelength Dependence of Refractive Indices of Flame Soot," *Proc. R. Soc. London, Ser. A*, **430**, pp. 577–591.
- [25] Lee, S. C., and Tien, C. L., 1981, "Optical Constants of Soot in Hydrocarbon Flames," *18th Symposium (International) on Combustion*, The Combustion Institute, Pittsburgh, pp. 1159–1166.
- [26] Gaydon, A. G., 1974, *The Spectroscopy of Flames*, 2nd ed., Chapman and Hall, London.
- [27] Dec, J., and Espey, C., 1998, "Chemiluminescence Imaging of Autoignition in a DI Diesel Engine," SAE Paper No. 982685.
- [28] Wersborg, B. L., Fox, L. K., and Howard, J. B., 1975, "Soot Concentration and Absorption Coefficient in a Low-Pressure Flame," *Combust. Flame*, **24**, pp. 1–10.
- [29] Vaglieco, B. M., Merola, S. S., D'Anna, A., and D'Alessio, A., 2002, "Spectroscopic Analysis and Modeling of Particulate Formation in a Diesel Engine," *J. Quant. Spectrosc. Radiat. Transf.*, **73**, pp. 443–450.
- [30] D'Anna, A., Violi, A., D'Alessio, A., and Sarofim, A. F., 2001, "A Reaction Pathway for Nanoparticle Formation in Rich Premixed Flames," *Combust. Flame*, **127**, pp. 1995–2003.
- [31] Bjorseth, A., 1985, *Handbook of Polycyclic Aromatic Hydrocarbons*, Marcel Dekker, New York.
- [32] Glassman, I., 1996, *Combustion*, 3rd ed., Academic Press, New York.
- [33] Richter, H., Howard, J. B., 2000, "Formation of Polycyclic Aromatic Hydrocarbons and Their Growth to Soot—A Review of Chemical Reaction Pathways," *Prog. Energy Combust. Sci.*, **26**, pp. 565–608.
- [34] Kitsopanis, I., 2004, "Experimental and Computational Study of Soot Formation Under Diesel Engine Conditions," Ph.D. thesis, Department of Mechanical Engineering, MIT, July, available at <http://libraries.mit.edu/>
- [35] Harris, S. J., and Weiner, A. M., 1983, "Determination of the Rate Constant for Soot Surface Growth," *Combust. Sci. Technol.*, **32**, pp. 267–275.
- [36] Wersborg, B. L., and Howard, J. B., 1975, "Soot Concentration and Absorption Coefficient in a Low-Pressure Flame," *Combust. Flame*, **24**, pp. 1–10.